WARMINGUP

Innovatief Duurzaam Warmtecollectief

Clogging in high temperature storage wells

Modeling the effect of high temperature

door
John van Esch
10 augustus 2022

Clogging in high temperature storage wells

Deltares

Auteur
John van Esch

10 augustus 2022

Kwaliteitsborgers
Hans van Meerten, Ivo Pothof, Johan Valstar

Dit project is uitgevoerd als onderdeel van het Innovatieplan WarmingUP. Dit is mede mogelijk gemaakt door subsidie van de Rijksdienst voor Ondernemend Nederland (RVO) in het kader van de subsidieregeling Meerjarige Missiegedreven Innovatie Programma's (MMIP), bij RVO bekend onder projectnummer TEUE819001.
WarmingUP geeft invulling aan MMIP-4 – Duurzame warmte en koude in gebouwde omgeving en levert daarmee een bijdrage aan Missie B – Een CO_2-vrije gebouwde omgeving in 2050.

Projectnummer
11205160-002

Keywords
Opslag, hoge temperatuur, verstopping, model

Jaar van publicatie
2022

Meer informatie
John van Esch
T 06 46552906
E john.vanesch@deltares.nl

Content

1 Introduction

High temperature aquifer thermal storage (HT-ATES) stores energy in the subsurface and makes use of extraction and infiltration of groundwater via wells. In such well applications, well plugging is a phenomenon that poses a risk to the sustainability of the energy storage system. In recent decades, a great deal of research has been carried out into the risk of well clogging for the drinking water production. For the extraction and infiltration of hot water in the groundwater system, the control of well clogging is also important. This WarmingUP sub-study addresses the question whether the risk of clogging is larger or smaller for HTO wells at higher temperatures, whether clogging occurs to the same extent or whether additional requirements must be imposed compared to existing guidelines for drinking water production. This report presents the first step of the research program on clogging processes in unconsolidated aquifers near high temperature storage wells. This report focusses on the effect of the temperature on the behavior of colloidal particles during injection. The effect of the release of colloidal particles near the production well is also an important aspect, but is not addressed in this report.

The clogging mechanism involves the transport and deposition of colloidal particles in saturated porous media. This physico-chemical filtration is also important for river bed filtration and deep-bed granular filtration in water treatment for instance. Colloid filtration models are used to simulate the deposition of colloids, viruses and bacteria. Classical models are based on the steady state particle transport equation without diffusion and apply to the first stage of the clogging process only.

Section 2 presents such a filtration model as explained by De Zwart (2007) that includes a contact efficiency term. Section 3 collects expressions for the single-collector contact efficiency in physico-chemical particle filtration that were proposed by Yao et al. (1971), Rajagopalan and Tein (1976) and Tufenkji and Elimelech (2004). The contact efficiency is calculated as a sum of individual transport mechanisms: Brownian diffusion, interception and gravitational sedimentation. Diffusion by Brownian motion that results in contact with the collector grains is the dominant process for particles with diameters smaller than 1 µm. For larger diameters interception and gravitational sedimentation become more important. Interception takes place when particles that move along a streamline come into contact with the collector grains. Particles with densities higher than the fluid, in which they are transported, settle on the collector due to gravitational sedimentation.

Section 4 proposes an extended filtration model that adds constitutive relations for fluid viscosity and density as a function of temperature. The model solves the flow equation that includes a damage function. This damage function scales the hydraulic conductivity as a function of deposited particle concentration. As a result, the hydraulic head in a groundwater abstraction well will be lower if clogging occurs for the case in which the abstraction rate is the same. However, for a situation in which the head in the abstraction well is controlled, the abstraction rate will decrease. This will affect the collector efficiency and the rate by which clogging takes place. Next the transport equation for the suspended particles is solved. The flow velocity and particle dispersion follow from the solution of the flow, the contact efficiency term relates to the flow velocity. The concentration of decomposed particles follows from the solution of a third equation and this concentration is used for calculating the damage function in the first equation. Section 5 collects the results of a series of model simulations. The impact of temperature is outlined by a single simulation that needs to be checked by laboratory experiments. Section 6 presents the conclusions and outlines future research.

2 Filtration model

2.1 Transport equation

Filtration models that are used to describe micro removal in porous media often predict an exponential decrease in micro-biological particle concentration with travel distance. The models are based on a one-dimensional particle mass balance that include first order particle decomposition kinetics. This equation reads:

$$\frac{\partial}{\partial t}(nc)+\frac{\partial}{\partial x}(uc)\frac{\partial^2}{\partial x^2}(Dc)+\lambda uc=0, \qquad \frac{\partial}{\partial t}(\sigma)-\lambda uc=0$$

Here time t (s) and space x (m) are independent variables that denote time and space. Concentration of the suspended material c (kg/m^3) and the concentration of deposited material σ (m^3/m^3) are chosen as primary variable. The Darcy velocity is given by u (m/s), the particle diffusion coefficient by D (m^2/s) and porosity is denoted as n (-). The filter coefficient λ (1/m) is an empirical filtration coefficient, which ranges from $0.001\,\mathrm{m}^{-1}$ to $0.1\,\mathrm{m}^{-1}$ and couples both equations. It transfers suspended material (particles) to deposited material (collector grains). The filter coefficient (not used in this article) relates to the decomposition rate k_d (1/s) as $k_d = v\lambda$, where the interstitial fluid velocity v (m/s) follows from the Darcy velocity as: $v = u/n$.
If the assumption is made that particle diffusion is negligible, groundwater flow is in-compressible, subsurface porosity changes are small and the change of suspended concentration due to deposition is negligible, then the one-dimensional particle mass balance equation can be rewritten as:

$$\frac{\partial c}{\partial x}+\lambda c=0, \qquad \frac{\partial \sigma}{\partial t}-\lambda uc=0$$

Imposing initial conditions:

$$c=0, \quad \sigma=0 \qquad \text{for} \quad 0\le x\le L \qquad \text{and} \qquad t=0$$

and boundary conditions at the inflow boundary:

$$c=\bar{c}, \qquad \text{for} \quad x=0$$

provides an analytic solution, which reads:

$$c=\bar{c}\exp(-\lambda x), \quad \sigma=\bar{c}\lambda u\exp(-\lambda x)t$$

This expression holds for a constant specific discharge and filtration coefficient and it must be noted that this filtration formulation can only be used in early states of clogging as the concentration of deposited material grows to infinity in time.
The filtration coefficient can be related to porosity n (-), collector efficiency $\alpha_c\eta$ (-) and the grain size diameter d_g (m) as:

$$\lambda=\frac{3(1-n)}{2d_g}\alpha_c\eta$$

The collector (removal) efficiency follows from the empirical collision efficiency α_c (-) and the collision probability (or collector contact efficiency) η (-). Under most conditions the collector efficiency is lower than the contact efficiency due to repulsive colloidal interactions between particles and collector grains Tufenkji and Elimelech (2004)). The collision efficiency expresses the number of particles depositing on the collector surface relative to the number of particles colliding with the collector. The collision probability (also written as η_p or η_0) follows from the number of particles colliding with the collector surface relative to the total number of particles approaching the collector (De Zwart (2007)). Column experiments are often used to determine the collision efficiency or attachment efficiency as current theories are in-adequate. The next section provides some expressions for the collector contact efficiency.

2.2 Collector contact efficiency

The equation for the collector contacts efficiency is given by:

$$\eta = \eta_d + \eta_i + \eta_g$$

where η_d (-) is the efficiency due to transport by diffusion, η_i (-) denotes the efficiency due to transport by interception and η_g (-) represents the efficiency due to gravitational sedimentation. Dimensionless parameters (aspect ratio, Peclet number, gravity number, London number, Van der Waals number, (an additional) gravitational number and attraction number) that govern particle filtration are presented first.

The aspect ratio N_r relates the particle diameter d_p (m) to the collector diameter d_g (m) and is given by:

$$N_r = \frac{d_p}{d_g}$$

The Peclet number N_{pe} that expresses the ratio of convective transport to diffusive transport D (m^2/s) reads:

$$N_{pe} = \frac{v d_g}{D}$$

where v (m/s) denotes liquid pore velocity and D (m^2/s) Brownian diffusion. The Brownian diffusion coefficient follows from the Stokes-Einstein equation as:

$$D = \frac{k_b T}{3\pi\mu d_p}$$

where $k_b = 1.3806 \cdot 10^{-23}$ J/K is Bolzmann's constant, μ (Pas) denotes the dynamic viscosity of the liquid and T (K) expresses the absolute temperature. The ratio of particle settling velocity and flow velocity is expressed by the gravity number N_g, which is given by:

$$N_g = \frac{d_p^2 \left(\rho_p - \rho_l\right) g}{18 \mu v}$$

where ρ_p $(\mathrm{kg/m^3})$ is the particle density, ρ_l $(\mathrm{kg/m^3})$ expresses the liquid density and the gravitational acceleration is given by g $(\mathrm{m/s^2})$. This expression holds for $\rho_p - \rho_l > 0$.
The London number N_{lo} represents the Van der Waals attractive force between collector and particle as:

$$N_{lo} = \frac{4A}{9\pi\mu v d_p^2}$$

Here, the Hamaker constant A is set to 10^{-20} J. Van der Waals interaction energy to the particle thermal energy N_w reads:

$$N_w = \frac{A}{k_b T}$$

This number can be used for an alternative formulation of the collector efficiency due to gravitational sedimentation.
The attraction number represents the influence of the attractive Van der Waals force and flow velocity as:

$$N_a = \frac{A}{3\pi\mu v d_p^2}$$

The dimensionless parameters will be used next to compute the collector efficiency. Yao et al. (1971) considers diffusion, interception and sedimentation and formulates the collision probability as:

$$\eta_{ya} = 3.94 A_s^{2/3} N_{pe}^{-2/3} + \tfrac{3}{2} N_r^2 + N_g$$

Rajagopalan and Tein (1976) extend this formulation and include hydrodynamic interactions and the effect of van der Waals attraction on Brownian diffusion.

$$\eta_{ra} = 4A_s^{1/3} N_{pe}^{-2/3} + A_s N_{lo}^{1/8} N_r^{15/8} + 3.38 \cdot 10^{-3} A_s N_g^{1.2} N_r^{-0.4}$$

The collision probability according to Tufenkji and Elimelech (2004) reads:

$$\eta_{tu} = 2.4 A_s^{1/3} N_r^{-0.081} N_{pe}^{-0.715} N_w^{0.052} + 0.55 A_s N_r^{1.675} N_a^{0.125} + 0.22 N_r^{-0.24} N_g^{1.11} N_w^{0.053}$$

In this expression incorporating Van der Waals attraction and hydrodynamic forces are included in all three mechanisms. The equation is based on a numerical solution of the convection-diffusion equation with all particle-removal mechanisms and interaction forces considered.
The Happel correction factor A_s (-), which is used by all formulations, depends on porosity n (-) and follows from:

$$A_s = \frac{2\left(1-\gamma^5\right)}{2-3\gamma+3\gamma^5-2\gamma^6}$$

where $\gamma = \left(1-n\right)^{1/3}$.

3 Filtration model simulations

3.1 Filtration simulation

Error! Reference source not found. shows the outcome of a steady state filtration simulation without dispersion and compares the numerical solution (solid lines) to the analytical solution (dashed lines). The numerical discretization sets: $\Delta x = 0.01\,\mathrm{m}$, $\Delta t = 5.0\,\mathrm{s}$ and applies a fully implicit schema;
$\theta = 1.0$. Model parameters are given by: $T = 15.0\,\mathrm{C}$, $u(x,t) = 1.28 \cdot 10^{-4}\ \mathrm{m/s}$ and $D = 0.0\,\mathrm{m}^2/\mathrm{s}$. Initial conditions read: $c(x,0) = 0.0\,\mathrm{kg/m}^3$ and boundary conditions impose a fixed concentration at the inflow site: $c(0,t) = 1.0\,\mathrm{kg/m}^3$.

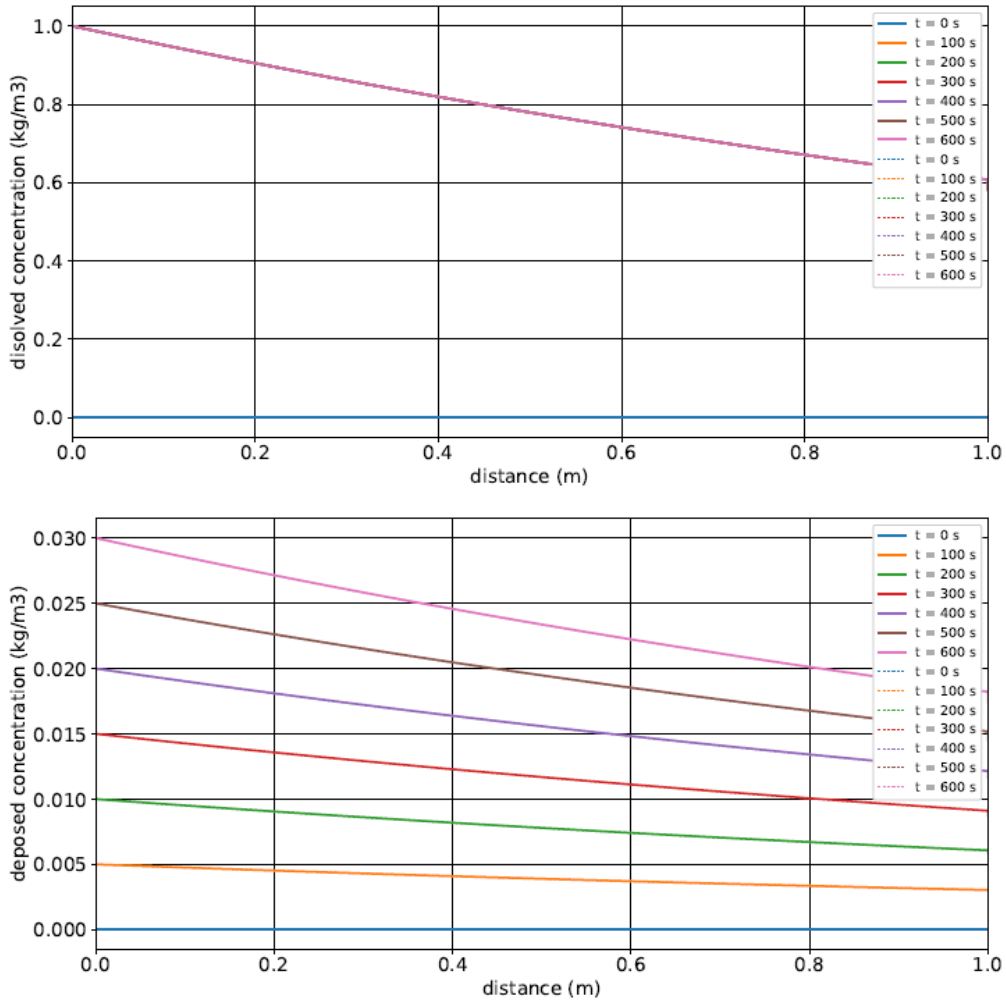

Figure 3-1 Steady state filtration without dispersion.

3.2 Collision probability simulation

In this subsection three filtration tests are simulated in a porous medium with collector diameter $d_g = 2 \cdot 10^{-4}$ m, porosity $n = 0.25$ and intrinsic permeability $\kappa = 3.25679 \cdot 10^{-11} \mathrm{m}^2$. The empirical collision efficiency α_c is set to 1.

A head loss per unit length $i = 1$ is chosen in the first simulation where the temperature T is set to $283.0\ \mathrm{K}$. Under this condition the liquid density ρ_l equals $999.86\ \mathrm{kg/m^3}$ and the dynamic viscosity of the fluid ν is $1.314 \cdot 10^{-3}\ \mathrm{Pas}$. The Darcy velocity $u\ (\mathrm{m/s})$ follows from:

$$u = Ki$$

where $K\ (\mathrm{m/s})$ denotes hydraulic conductivity. The hydraulic conductivity relates to the intrinsic permeability, the density of the liquid phase, the dynamic viscosity of the fluid and the gravitational acceleration coefficient $g\ (\mathrm{m/s^2})$, which was set to $9.81\ \mathrm{m/s^2}$. This relation can be written as:

$$K = \frac{\kappa \rho g}{\mu}$$

The actual velocity $v\ (\mathrm{m/s})$ is obtained from the Darcy velocity as: $v = u / n$. By using the given parameter set the actual velocity reads: $v = 9.72 \cdot 10^{-4}\ \mathrm{m/s}$ and the Darcy velocity $u = 2.43 \cdot 10^{-4}\ \mathrm{m/s}$ for the first test. Figure 3-2 compares the expressions for the collision probability for the first test and varies the particle diameter between $d_p = 10^{-7}\ \mathrm{m}$ and $d_p = 10^{-4}\ \mathrm{m}$. Brownian diffusion, interception and gravitational sedimentation are given for the model presented by Tufenkji and Elimelech (2004). The influence of the hydrodynamic viscous interaction becomes more significant for increasing particle size.

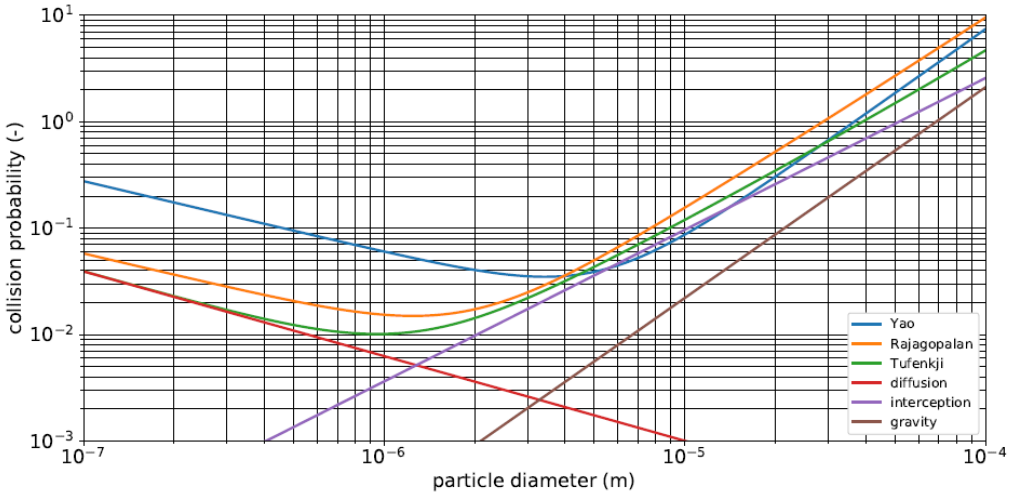

Figure 3-2 Collision probability as a function of particle diameter ($T = 15°\mathrm{C}, u = 21$ m/d).

In the second test the temperature is set to $353.0\ \mathrm{K}$. This changes the dynamic viscosity and the density of the fluid. The dynamic viscosity of pure water as a function of temperature (Diersch (2004)) is given by:

$$\mu = 2.4318 \cdot 10^{-5} \cdot 10^{247.8/(T-140.0)}$$

The density of water relates to temperature and Diersch (2004) proposes a six order Taylor expansion which is approximated here by:

$$\rho_l = 10^3 + 6.76 \cdot 10^{-2} (T - 273) - 8.99 \cdot 10^{-3} (T - 273)^2 + 9.14 \cdot 10^{-5} (T - 273)^3$$

According to these relations the second test sets the dynamic viscosity $\nu = 3.542 \cdot 10^{-4}$ Pas and liquid density $\rho_l = 994.67 \text{ kg/m}^3$. By decreasing the head loss per unit length however, the velocity is kept the same as in the first experiment; $v = 84 \text{ m/d}$, $u = 21 \text{ m/d}$. Figure 3-3 presents the collision probability as a function of particle diameter at $80°\text{C}$ and a decreased head loss.

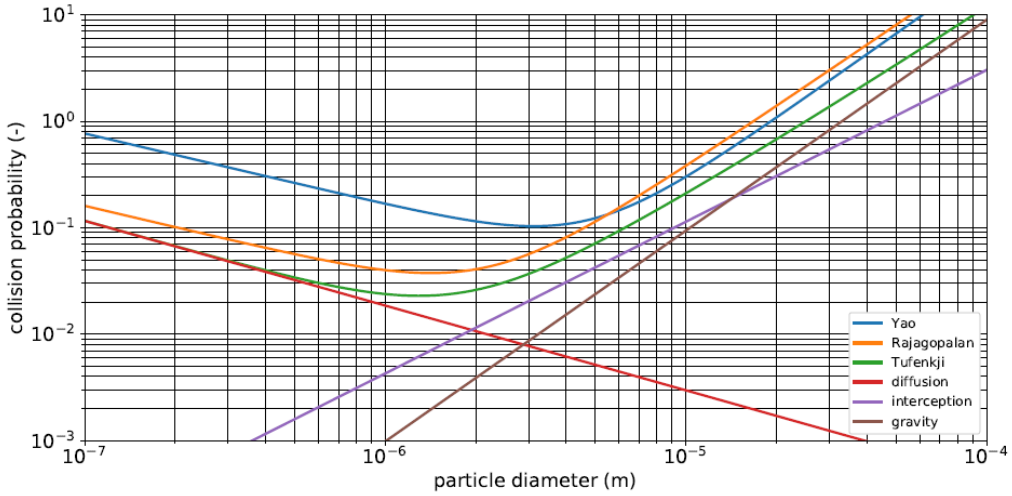

Figure 3-3 Collision probability as a function of particle diameter ($T = 80°\text{C}, u = 21$ m/d).

As the viscosity of water decreases at higher temperatures, larger flow velocities can be maintained at equivalent hydraulic head loss near the production well ($i = 1$). In this case the velocity can be increased by a factor 3.7 up to $v = 310 \text{ m/d}$ and $u = 78 \text{ m/d}$.

Figure 3-4 Collision probability as a function of particle diameter ($T = 80°\text{C}, u = 78$ m/d). presents the collision probability for the third test as a function of particle diameter at $80°\text{C}$ and an increased filter velocity.

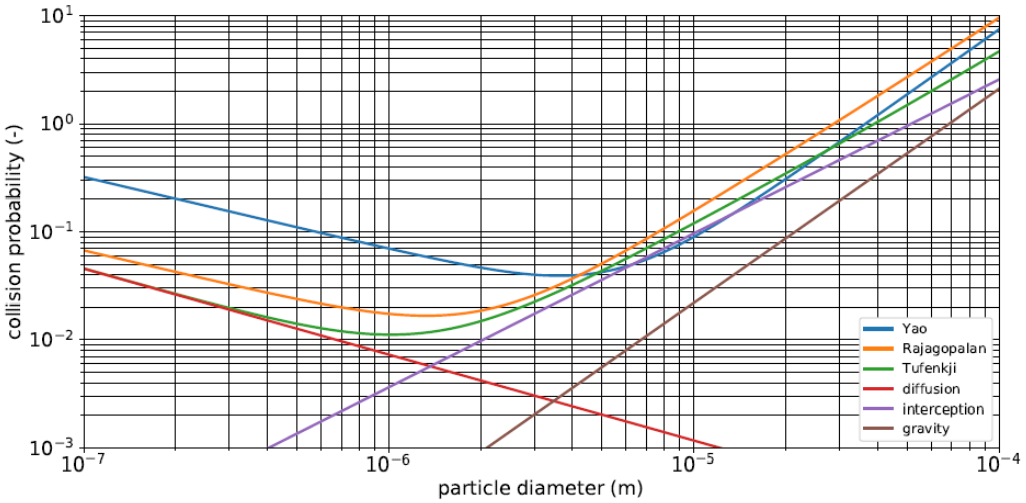

Figure 3-4 Collision probability as a function of particle diameter ($T = 80°\text{C}, u = 78$ m/d).

Table 3-1 and Table 3-2 present filtration model parameters for particle diameters $d_p = 10^{-6}$ m and $d_p = 2 \cdot 10^{-5}$ m. Table 3-1 compares the outcome of the first and second test for equivalent Darcy velocity $u = 21$ m/d.

Table 3-1 Filtration model parameters, equivalent velocity.

number	$d_p = 10^{-6}$ m $u = 21$ m/d $T = 15$°C	$d_p = 2 \cdot 10^{-5}$ m $u = 21$ m/d $T = 15$°C	$d_p = 10^{-6}$ m $u = 21$ m/d $T = 80$°C	$d_p = 2 \cdot 10^{-5}$ m $u = 21$ m/d $T = 80$°C
μ	1.31E-03	1.31E-03	3.54E-04	3.54E-04
ρ_l	1.00E+03	1.00E+03	9.95E+02	9.95E+02
A_s	1.15E+02	1.15E+02	1.15E+02	1.15E+02
D	3.15E-13	1.58E-14	1.46E-12	7.30E-14
N_r	5.00E-03	1.00E-01	5.00E-03	1.00E-01
N_{pe}	6.16E+05	1.23E+07	1.33E+05	2.66E+06
N_g	7.04E-04	2.82E-01	2.62E-03	1.05E+00
N_{lo}	1.11E-03	2.77E-06	4.11E-03	1.03E-05
N_{vdw}	2.56E+00	2.56E+00	2.05E+00	2.05E+00
N_a	8.30E-04	2.08E-06	3.08E-03	7.70E-06
η_{ya}	1.36E-02	2.98E-01	3.83E-02	1.07E+00
η_{ra}	5.58E-03	5.21E-01	1.28E-02	1.39E+00
η_{tu}	5.25E-03	3.58E-01	9.41E-03	7.24E-01
λ_{ya}	7.63E+01	1.68E+03	2.15E+02	6.01E+03
λ_{ra}	3.14E+01	2.93E+03	7.21E+01	7.83E+03
λ_{tu}	2.95E+01	2.01E+03	5.30E+01	4.07E+03

The results in Table 3-2 indicate that the collector contact efficiency increases by a factor of 1.8 in case of high temperature storage at 80°C compared to the drinking water production case when the groundwater temperature is 15°C if Tufenkji and Elimelech (2004) model is adopted and small particle diameters of $d_p = 10^{-6}$ m are considered. For larger particle diameters ($d_p = 2 \cdot 10^{-5}$ m) the collector contact efficiency increases by a factor of 2.0.

Table 3-2 compares the first and third test where the near well head drop is equivalent $i = 1$ setting the Darcy velocity to 21 m/d for the drinking water production well and 78 m/d for the thermal storage system.

Table 3-2 Filtration model parameters, equivalent head drop

number	$d_p = 10^{-6}$ m $u = 21$ m/d $T = 15$°C	$d_p = 2 \cdot 10^{-5}$ m $u = 21$ m/d $T = 15$°C	$d_p = 10^{-6}$ m $u = 78$ m/d $T = 80$°C	$d_p = 2 \cdot 10^{-5}$ m $u = 78$ m/d $T = 80$°C
μ	1.31E-03	1.31E-03	3.54E-04	3.54E-04
ρ_l	1.00E+03	1.00E+03	9.95E+02	9.95E+02
A_s	1.15E+02	1.15E+02	1.15E+02	1.15E+02
D	3.15E-13	1.58E-14	1.46E-12	7.30E-14
N_r	5.00E-03	1.00E-01	5.00E-03	1.00E-01
N_{pe}	6.16E+05	1.23E+07	4.92E+05	9.83E+06
N_g	7.04E-04	2.82E-01	7.10E-04	2.84E-01
N_{lo}	1.11E-03	2.77E-06	1.11E-03	2.78E-06
N_{vdw}	2.56E+00	2.56E+00	2.05E+00	2.05E+00
N_a	8.30E-04	2.08E-06	8.35E-04	2.09E-06
η_{ya}	1.36E-02	2.98E-01	1.57E-02	3.01E-01
η_{ra}	5.58E-03	5.21E-01	6.03E-03	5.24E-01
η_{tu}	5.25E-03	3.58E-01	5.48E-03	3.58E-01
λ_{ya}	7.63E+01	1.68E+03	8.81E+01	1.69E+03
λ_{ra}	3.14E+01	2.93E+03	3.39E+01	2.94E+03
λ_{tu}	2.95E+01	2.01E+03	3.08E+01	2.01E+03

The results in Table 3-2 indicate that the collector contact efficiency hardly changes due to temperature differences if the head loss over a unit length remains the same.
These findings indicate that the risk of clogging for high temperature storage systems is larger than the risk of clogging in drinking water production wells in the case that the velocity of pore water remains the same. However, Tufenkji and Elimelech (2004) constructed their correlation equation for predicting single-collector efficiency at low temperatures and laboratory tests at high temperatures are needed to validate the application under these conditions. Furthermore, the empirical collision efficiency might change resulting in an altered filter coefficient. The table indicated a decrease in viscosity by a factor 3.7 and density decrease by less than 1% for the thermal storage case compared to the drinking water production case. The impact of high temperatures viscosity and liquid density will be studied in the next section.

4 Extended filtration model

The extended filtration model couples the flow equation, the transport equation for suspended particles and the box equation for deposited material and applies the collision probability function that was proposed by Tufenkji and Elimelech (2004). The permeability of the porous media is reduced by a damage function. This section presents a one-dimensional finite difference formulation. The appendix verifies the outcome of the sub-models with analytical solutions and presents a two-dimensional finite element formulation.

4.1 Flow equation

The actual pore velocity $v\ (\mathrm{m/s})$ follows from a one-dimensional flow equation (Van Esch (2010)) that is given by:

$$S\frac{\partial\phi}{\partial t}-\frac{\partial}{\partial x}\left(kK\frac{\partial\phi}{\partial x}\right)=0$$

as: $v=-kK/n\cdot\partial\phi/\partial x$. In this flow equation formulation $S\ (1/\mathrm{m})$ is the storage coefficient, $\phi\ (\mathrm{m})$ denotes hydraulic head, k (-) is known as damage function and $K\ (\mathrm{m/s})$ express the hydraulic conductivity. This damage function scales the hydraulic conductivity as a function of deposited particle concentration. Specific discharge $u\ (\mathrm{m/s})$ relates to pore velocity as: $u=nv$ where n (-) is porosity. Initial conditions are given by:

$$\phi=0 \qquad \text{for} \quad 0\le x\le L \qquad \text{and} \qquad t=0$$

and boundary conditions at the inflow and outflow boundary read:

$$\phi=\bar{\phi}_0 \qquad \text{for} \quad x=0, \quad \phi=\bar{\phi}_1 \qquad \text{for} \quad x=1$$

A first order damage function that reduces the permeability due to deposition of particles is given by:

$$k=\frac{1}{1+\beta\sigma}$$

where β (-) is the formation damage coefficient (De Zwart (2007)).

A finite difference discretisation will be used to solve the flow equation. It applies a six-point molecule (central differencing in space and time) and Crank-Nicholson time integration. This finite difference approximation reads:

$$S\frac{\phi_j^{n+1}-\phi_j^n}{\Delta t}-\theta\left(k_j^{n+1}K\frac{\phi_{j+1}^{n+1}-2\phi_j^{n+1}+\phi_{j-1}^{n+1}}{\Delta x^2}\right)-(1-\theta)\left(k_j^nK\frac{\phi_{j+1}^n-2\phi_j^n+\phi_{j-1}^n}{\Delta x^2}\right)=0$$

The amplification factor of the method can be written as:

$$\rho=\frac{1+(1-\theta)\lambda(\cos\xi-1)}{1-\theta\lambda(\cos\xi-1)}$$

where the diffusion parameter follows from: $\lambda = 2kK\Delta t / S\Delta x^2$. The method is unconditionally stable for $0.5 \le \theta \le 1$ and the explicit approach ($\theta = 0$) is stable under the conditions $0 \le \lambda \le 1$ or

$$\Delta t \le \frac{S\Delta x^2}{2kK}$$

A θ-factor close to 0.5 is preferable for accuracy as can be shown by a Taylor series expansion around the point (j, n)

$$S\frac{\partial \phi}{\partial t} - \frac{\partial}{\partial x}\left(kK\frac{\partial \phi}{\partial x}\right) = -\tfrac{1}{2}S\Delta t\frac{\partial^2 c}{\partial t^2} + \tfrac{1}{12}kK\Delta x^2\frac{\partial^4 c}{\partial x^4}$$

The algebraic set of equations that needs to be solved reads:

$$a\phi_{j-1}^{n+1} + b\phi_j^{n+1} + c\phi_{j+1}^{n+1} = d$$

where:

$$a = -\theta\Delta t\frac{k_j^{n+1}K}{\Delta x^2},$$

$$b = S + 2\theta\Delta t\frac{k_j^{n+1}K}{\Delta x^2},$$

$$c = -\theta\Delta t\frac{k_j^{n+1}K}{\Delta x^2},$$

$$d = S\phi_j^n + (1-\theta)\Delta t\left(k_j^n K\frac{\phi_{j+1}^n - 2\phi_j^n + \phi_{j-1}^n}{\Delta x^2}\right)$$

4.2 Transport equation

The transport equation for the suspended and deposited material (Tufenkji et al. (2003)) is given by:

$$n\frac{\partial c}{\partial t} + u\frac{\partial c}{\partial x} - D\frac{\partial^2 c}{\partial x^2} + \lambda uc = 0, \qquad \frac{\partial \sigma}{\partial t} - \lambda uc = 0$$

Initial conditions are given by:

$$c = 0, \quad \sigma = 0 \qquad \text{for} \quad 0 \le x \le L \qquad \text{and} \qquad t = 0$$

and boundary conditions at the inflow boundary read:

$$c = \bar{c} \qquad \text{for} \quad x = 0 \qquad \text{and} \quad c = 0 \qquad \text{for} \quad x \to \infty$$

A finite difference discretization will also be used to solve the convection-diffusion equation for the suspended material. This discretization applies a six-point molecule and Crank-Nicholson time integration. This finite difference approximation is written as:

$$n\frac{c_j^{n+1}-c_j^n}{\Delta t}+\theta\left(u_j^{n+1}\frac{c_{j+1}^{n+1}-c_{j-1}^{n+1}}{2\Delta x}-D\frac{c_{j+1}^{n+1}-2c_j^{n+1}+c_{j-1}^{n+1}}{\Delta x^2}+\lambda_j^{n+1}u_j^{n+1}c_j^{n+1}\right)+$$
$$(1-\theta)\left(u\frac{c_{j+1}^{n}-c_{j-1}^{n}}{2\Delta x}-D\frac{c_{j+1}^{n}-2c_j^{n}+c_{j-1}^{n}}{\Delta x^2}+\lambda_j^{n}u_j^{n}c_j^{n}\right)=0$$

For computations of in-compressible flow, without diffusion and constant porosity an alternative schema is used:

$$\frac{c_j^{n+1}-c_{j-1}^{n+1}}{\Delta x}+\lambda_j^{n+1}c_j^{n+1}=0$$

This forward in time integration is preferred over the central in time integration because it does not show numerical wiggles or short waves with wave lengths $2\Delta x$. However, wiggles do not grow in time and persist in steady state so they are not related to instability but indicate in fact numerical in-accuracy (Vreugdenhill (1989)).

The ordinary differential equation for the deposited material that applies Crank-Nicholson time integration reads:

$$\frac{\sigma_j^{n+1}-\sigma_j^n}{\Delta t}-\theta\left(\lambda_j^{n+1}u_j^{n+1}c_j^{n+1}\right)-(1-\theta)\left(\lambda_j^{n}u_j^{n}c_j^{n}\right)=0$$

The amplification factor for the convection-diffusion model can be written as:

$$\rho=\frac{1+(1-\theta)\lambda(\cos\xi-1)-(1-\theta)iN_{cr}\sin\xi}{1-\theta\lambda(\cos\xi-1)+\theta iN_{cr}\sin\xi}$$

where the diffusion parameter reads: $\lambda=2D\Delta t/n\Delta x^2$ and the Courant number is given by $N_{cr}=u\Delta t/u\Delta x$. The method is unconditionally stable for $0.5\le\theta\le1$ and the explicit approach ($\theta=0$) is stable under two conditions $N_{cr}^2\le\lambda\le1$, which can be rewritten as:

$$\Delta t\le\frac{n\Delta x^2}{2D}\quad\cap\quad\Delta t\le\frac{2nD}{u^2}$$

The restriction on the grid size holds if the condition $N_{pe}\le2$ is met, where $N_{pe}=|u\Delta x/D|$ denotes the cell Peclet number. A Taylor series expansion of the numerical schema to the point (j,n) gives:

$$n\frac{\partial c}{\partial t}+u\frac{\partial c}{\partial x}-D\frac{\partial^2 c}{\partial x^2}+\lambda uc=-\tfrac{1}{2}n\Delta t\frac{\partial^2 c}{\partial t^2}-\tfrac{1}{6}u\Delta x^2\frac{\partial^3 c}{\partial x^3}+\tfrac{1}{12}D\Delta x^2\frac{\partial^4 c}{\partial x^4}$$

The expansion reveals a numerical diffusion coefficient $D_n\ (\mathrm{m}^2/\mathrm{s})$ that can be written as:

$$D_n=\left(\theta-\tfrac{1}{2}\right)\frac{u^2}{n^2}\Delta t$$

For positive values ($\theta\ge\frac{1}{2}$) the method adds diffusion to the solution, which is inline with the stability analysis. The condition that total diffusion should be positive provides a restriction on the time step: $\Delta t<2nD/u^2$ for the explicit form. The procedure for selecting spatial and temporal discretization reads:

$$\Delta x \le \frac{2D}{u} \quad \cap \quad \Delta t \le \frac{n\Delta x^2}{2D}$$

The solution is most accurate for $\theta = \frac{1}{2}$. For this setting numerical diffusion disappears but other terms in the Taylor expansion still cause numerical errors. The condition $N_{pe} \le 2$ prevents over and undershoot problems (wiggles due to spatial inaccuracy). The algebraic set of equations that needs to be solved reads:

$$ac_{j-1}^{n+1} + bc_j^{n+1} + cc_{j+1}^{n+1} = d$$
$$ec_j^{n+1} + \sigma_j^{n+1} = f$$

where:

$$a = \theta\Delta t\left(-\frac{u_j^{n+1}}{2\Delta x} - \frac{D}{\Delta x^2}\right)$$

$$b = n + \theta\Delta t\left(\frac{2D}{\Delta x^2} + \lambda_j^{n+1}u_j^{n+1}\right)$$

$$c = \theta\Delta t\left(\frac{u_j^{n+1}}{2\Delta x} - \frac{D}{\Delta x^2}\right)$$

$$d = nc_j^n - (1-\theta)\Delta t\left(u_j^n\frac{c_{j+1}^n - c_{j-1}^n}{2\Delta x} - D\frac{c_{j+1}^n - 2c_j^n + c_{j-1}^n}{\Delta x^2} + \lambda_j^n u_j^n c_j^n\right)$$

$$e = -\theta\Delta t\left(\lambda_j^{n+1}u_j^{n+1}\right)$$

$$f = \sigma_j^n + (1-\theta)\Delta t\left(\lambda_j^n u_j^n c_j^n\right)$$

4.3 Coupling terms

The discrete value of the damage function k_j^n follows from the concentration of deposited material σ_j^n, which in its turn follows from the concentration of suspended material c_j^n. The Darcy velocity at the center of a finite difference cell j follows from the computed heads in the adjacent cells $j-1$ and $j+1$ as:

$$u_j^n = k_j^n K\frac{\phi_{j-1}^n - \phi_{j+1}^n}{2\Delta x}$$

This velocity supports the transport equation for the suspended material and is used in the computation of the collector efficiency. The damage function discretization is given by:

$$k_j^n = \frac{1}{1+\beta\sigma_j^n}$$

The filtration coefficient that was proposed in the previous section follows from:

$$\lambda_j^n = \frac{3(1-n)}{2d_g}\alpha_c\eta_j^n$$

The collision probability η_j^n depends on flow velocity.

5 Extended filtration model simulations

This section presents two coupled flow and filtration simulations where the collision probability model that was suggested by Tufenkji and Elimelech (2004) is used. The first case simulates clogging of a drinking water production well for which the collision probability was presented by **Error! Reference source not found.** and numerical values where collected in Table 3-1. The extended filtration model computes Darcy velocity $u = 2.43 \cdot 10^{-4}$ m/s and a filter coefficient $\lambda =$ 29.5 1/m that correspond to the preset values in the table as the collision efficiency was set to $\alpha = 0.1$ m. The second case simulates a high temperature storage system for which the collision probability was presented by Figure 3-2 and numerical values where collected in Table 3-2. Here the extended filtration model computes a Darcy velocity $u = 9.03 \cdot 10^{-4}$ m/s and a filter coefficient $\lambda = 30.8$ 1/m that also correspond to the tabulated data.

5.1 Drinking water production simulation

Figure 5-1 and Figure 5-2 present the outcome of the coupled flow and filtration simulation at low drinking water production temperatures $(T = 10°\mathrm{C})$. For this problem there is no analytical solution available. The collector contacts efficiency formula given by Tufenkji is used, with particle diameter $d_p = 10^{-6}$ m, particle density $\rho_p = 2650.0$, kg/m^3, collector diameter $d_g = 2 \cdot 10^{-4}$ m and collision efficiency $\alpha = 0.1$ m. The numerical schema uses: spatial increment $\Delta x = 0.005$ m, time step $\Delta t = 5.0$ s and weight factor $\theta = 0.55$. The set of model parameters reads: temperature $T = 10.0$ C, intrinsic permeability $\kappa = 3.26 \cdot 10^{11}$ m^2, liquid density $\rho_l = 999.87$ kg/m^3, dynamic viscosity $\mu = 1.314 \cdot 10^{-3}$ Pas, specific storativity $S = 10^{-4}$ 1/m, porosity $n = 0.25$, dispersivity $D = 2 \cdot 10^{-6}$ m^2/s and damage coefficient $\beta = 0.1$ m^3/kg. Initial conditions are given by: hydraulic head $\phi(x,0) = 0.0$ m and concentration dissolved particles $c(x,0) = 0.0$ kg/m^3. Boundary conditions impose a hydraulic head at both sides of the flow domain and set a constant dissolved particle concentration at the inflow side: left side head $\phi(0,t) = 1.0$ m,
right side head $\phi(1.0,t) = 0.0$ m and left side particle concentration $c(0,t) = 1.0$ kg/m^3.

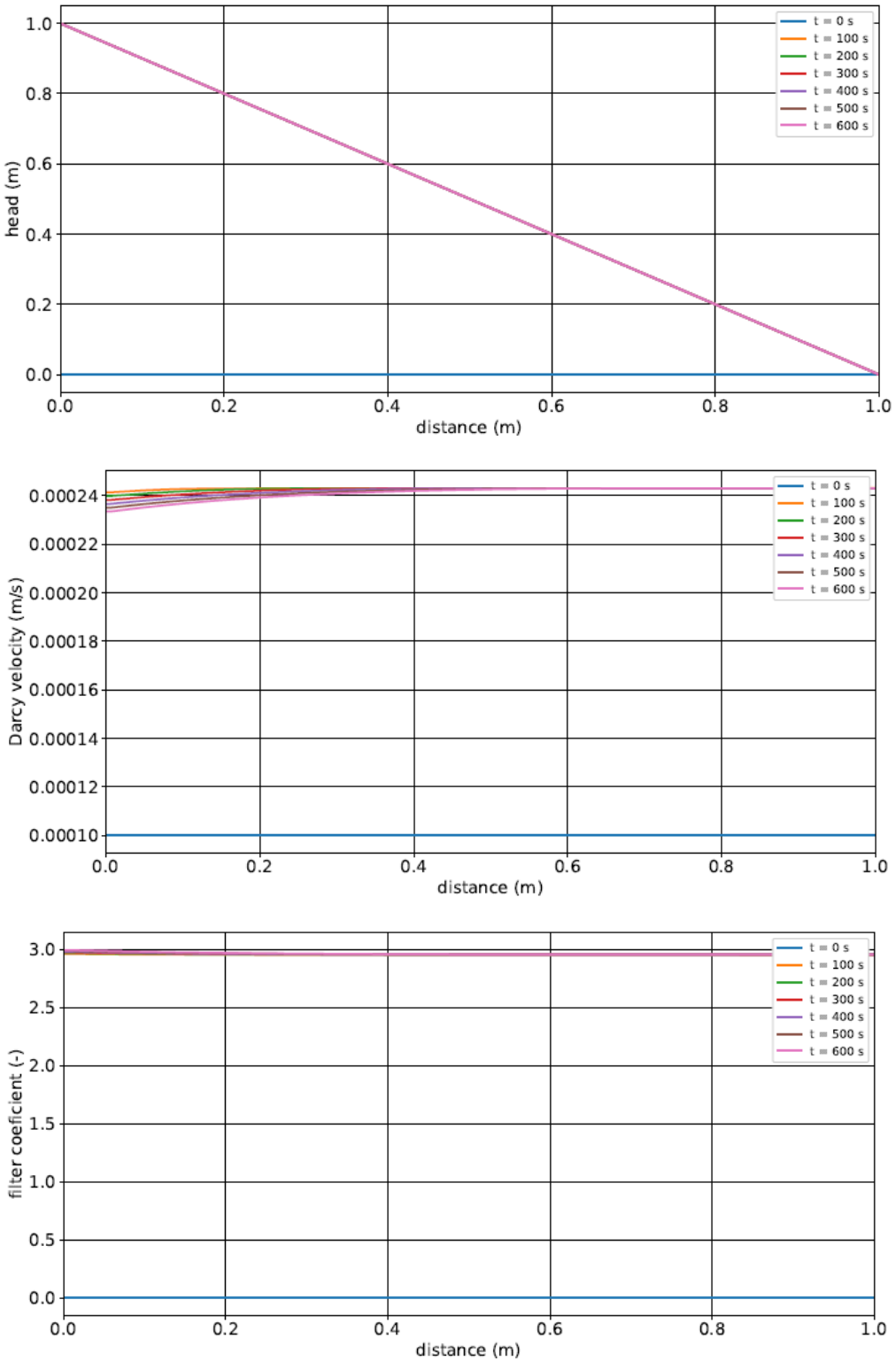

Figure 5-1 Coupled time dependent flow ($T = 15$°C).

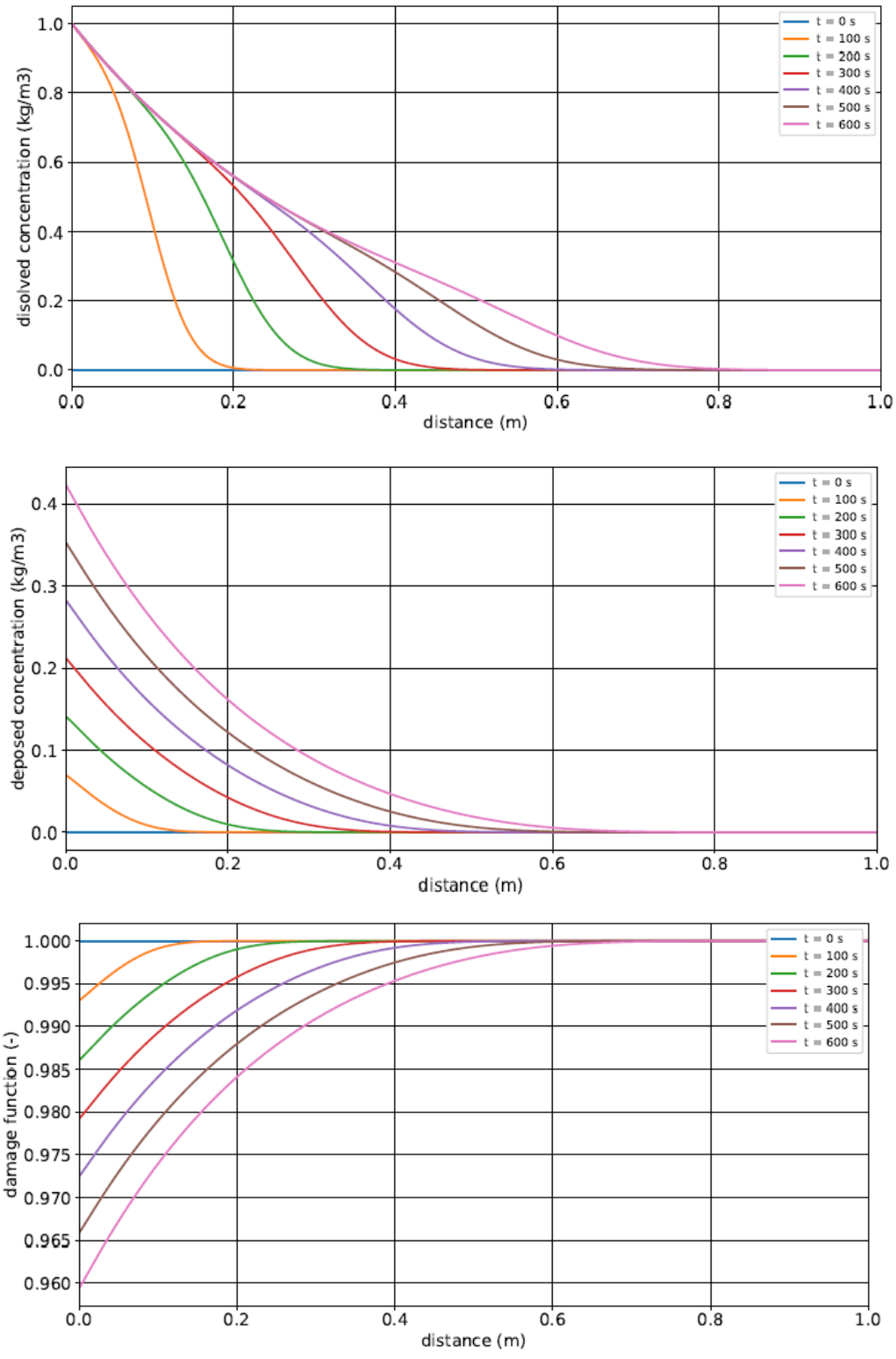

Figure 5-2 Coupled time dependent filtration ($T = 15$°C).

5.2 High temperature storage simulation

Figure 5-3 and Figure 5-4 show the outcome of a coupled flow and filtration simulation at high temperature storage conditions $(T = 80°\mathrm{C})$. The collector contact efficiency formula given by Tufenkji is used, with particle diameter $d_p = 10^{-6}\ \mathrm{m}$, particle density $\rho_p = 2650.0,\ \mathrm{kg/m^3}$, collector diameter $d_g = 2 \cdot 10^{-4}\ \mathrm{m}$ and collision efficiency $\alpha = 0.1\ \mathrm{m}$. The numerical schema uses: spatial increment $\Delta x = 0.005\ \mathrm{m}$, time step $\Delta t = 5.0\ \mathrm{s}$ and weight factor $\theta = 0.55$.
The set of model parameters reads: temperature $T = 80.0\ \mathrm{C}$, intrinsic permeability $\kappa = 3.26 \cdot 10^{11}\ \mathrm{m^2}$, liquid density $\rho_l = 994.67\ \mathrm{kg/m^3}$, dynamic viscosity $\mu = 3.5424 \cdot 10^{-4}\ \mathrm{Pas}$, hydraulic conductivity $K = 8.97 \cdot 10^{-4}\ \mathrm{m/s}$, specific storativity $S = 10^{-4}\ 1/\mathrm{m}$, porosity $n = 0.25$, dispersivity $D = 2 \cdot 10^{-6}\ \mathrm{m^2/s}$ and damage coefficient $\beta = 0.1\ \mathrm{m^3/kg}$. Initial conditions are given by: hydraulic head $\phi(x, 0) = 0.0\ \mathrm{m}$ and concentration dissolved particles $c(x, 0) = 0.0\ \mathrm{kg/m^3}$.
and boundary conditions impose a hydraulic head at both sides of the flow domain and set a constant dissolved particle concentration at the inflow side: left side head $\phi(0, t) = 1.0\ \mathrm{m}$, right side head $\phi(1.0, t) = 0.0\ \mathrm{m}$ and left side particle concentration $c(0, t) = 1.0\ \mathrm{kg/m^3}$.

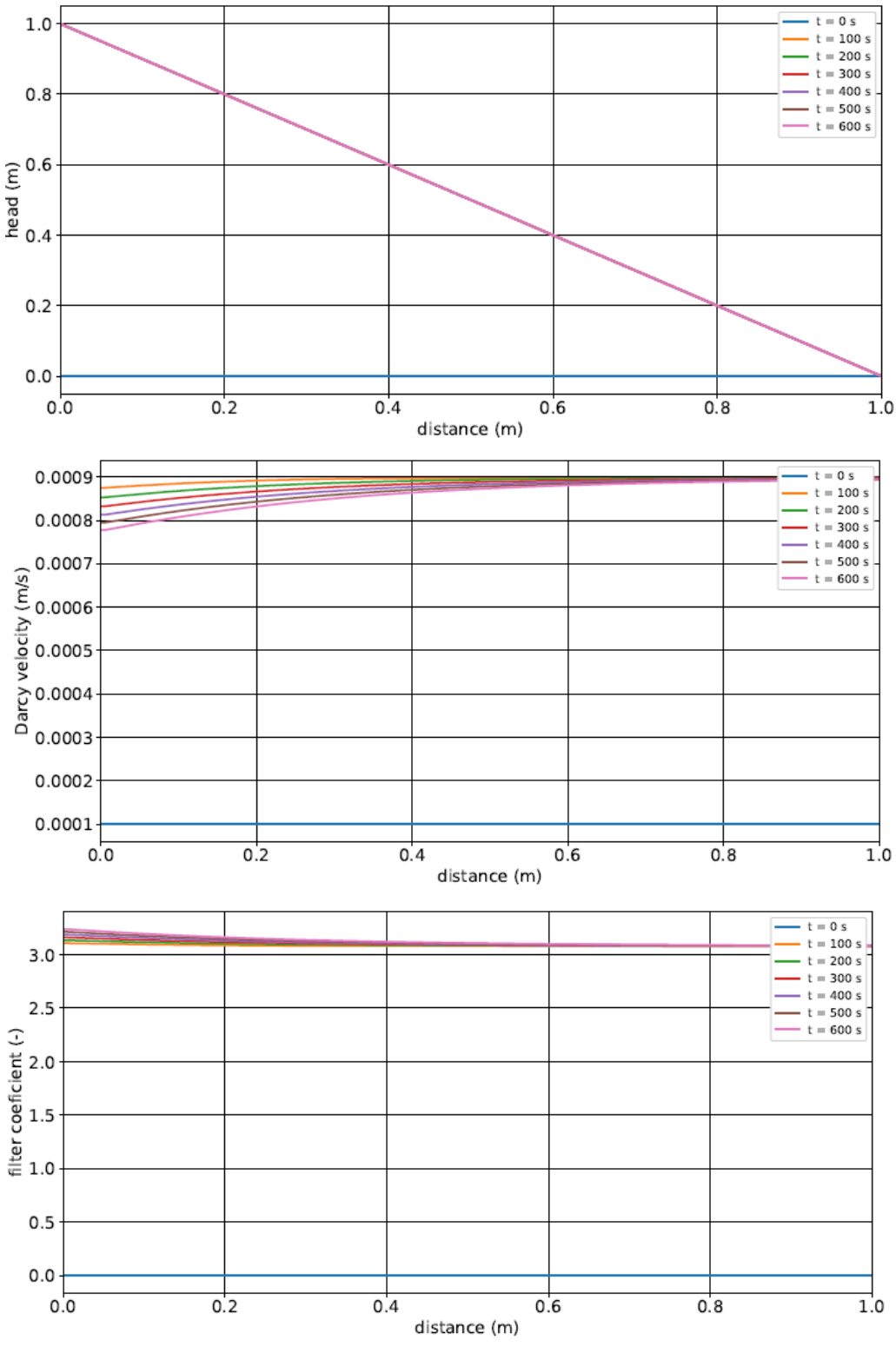

Figure 5-3 Coupled time dependent flow ($T = 80°$).

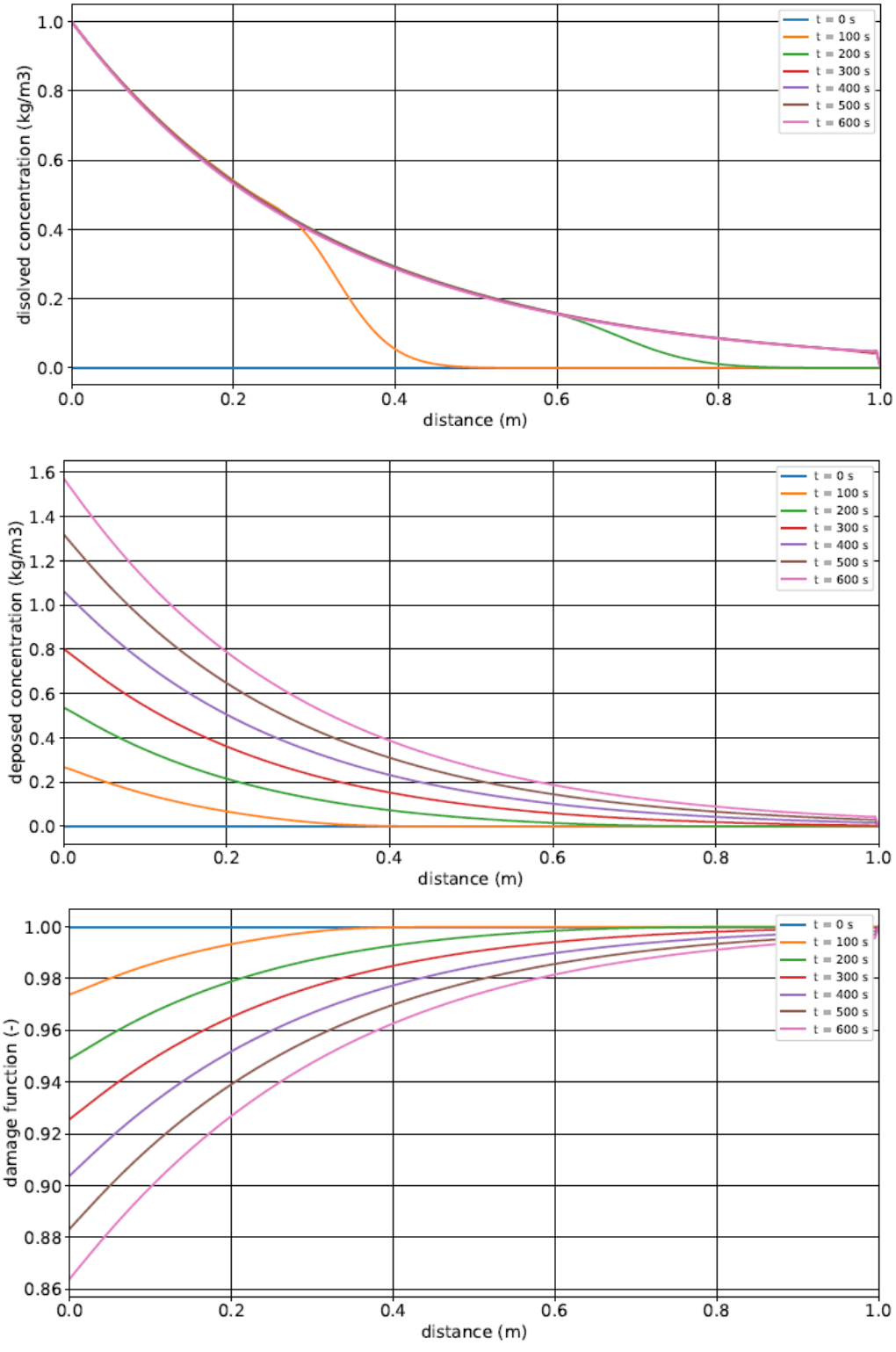

Figure 5-4 Coupled time dependent filtration ($T = 80$°C).

6 Conclusion

The extended filtration model that was presented in this report, adds constitutive relations for fluid viscosity and density as a function of temperature to the one-dimensional particle mass balance equation with first order deposition kinetics. The filter coefficient in this equation follows from a collector contact formulation that was presented by Tufenkji and Elimelech (2004). The flow velocity that is used in both the mass balance equation of the dissolved particle concentration and the collector contact formulation is obtained by solving the flow equation. For a prescribed head loss, the flow velocity depends strongly on the fluid density and viscosity. The flow equation includes a damage function that scales the hydraulic conductivity as a function of deposited particle concentration. The damage function models the clogging process as the permeability is reduced when particles are deposited. The deposed particle concentration follows from a third mass balance equation.

Figure 6-1 presents the collector contact efficiency or collision probability for a drinking water production well that operates at a temperature of $15℃$ at a near well filter velocity of $21\mathrm{m/d}$.

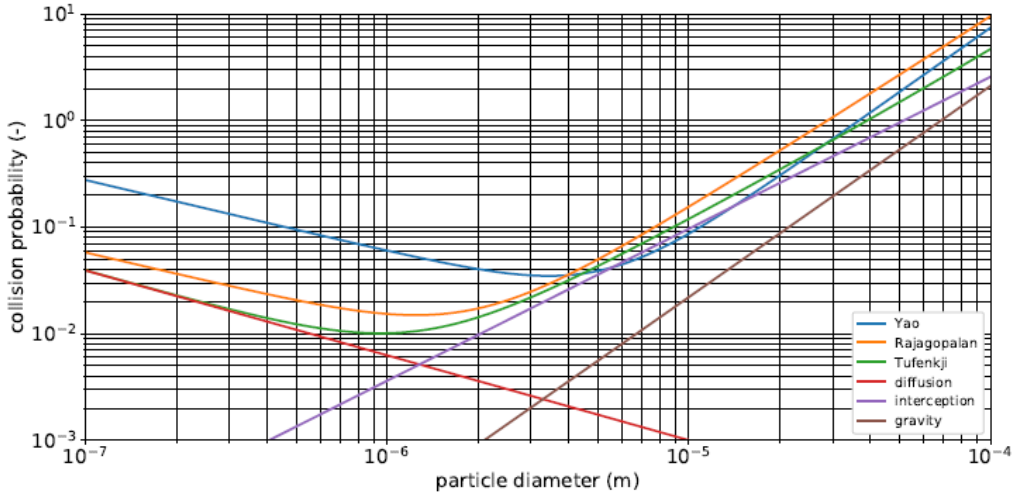

Figure 6-1 Collision probability for a drinking water production well.

Figure 6-2 presents the collector contact efficiency for a thermal storage system that operates at a temperature of $80℃$ and a near well filter velocity of $78\mathrm{m/d}$. The head drop per unit length for both the drinking water production case and the thermal storage system case was set to one. The increase in pore water velocity at higher temperatures results from the change in viscosity and fluid density. Porous media properties like grain size, particle densities and intrinsic permeability were identical for both cases.

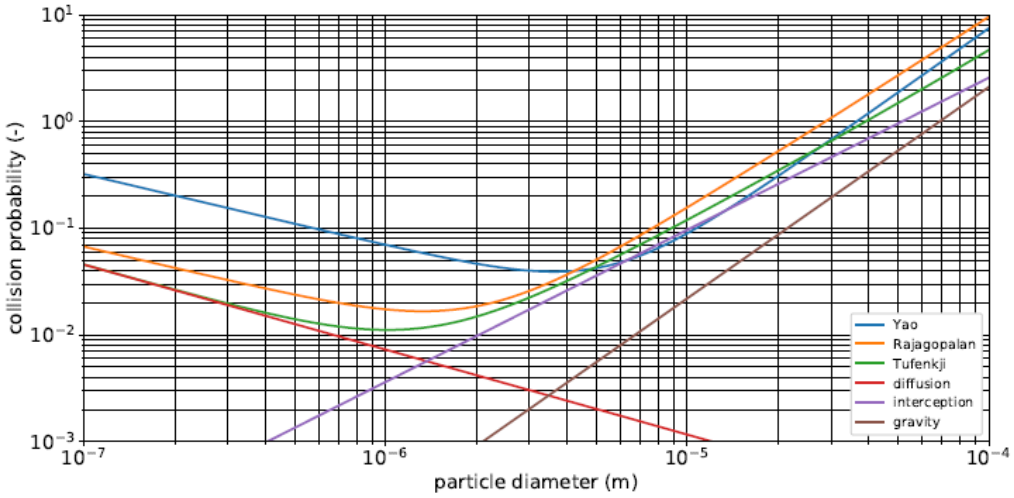

Figure 6-2 Collision probability for a thermal storage system.

The results indicate that the collector contact efficiency hardly changes due to temperature differences if the head loss over a unit length remains the same. However, Tufenkji and Elimelech (2004) constructed their correlation equation for predicting single-collector efficiency at low temperatures and laboratory tests at high temperatures are needed to validate the application under these conditions. Furthermore, the empirical collision efficiency might change resulting in an altered filter coefficient. For the 10 minute column test that was presented in this article, the extended filtration model simulation for hot water storage at $80℃$ shows that the concentration of deposed particles is about four times larger than the concentration of deposed particles for drinking water production at $10℃$ at the inlet point as can be seen in Figure 6-3 and Figure 6-4.

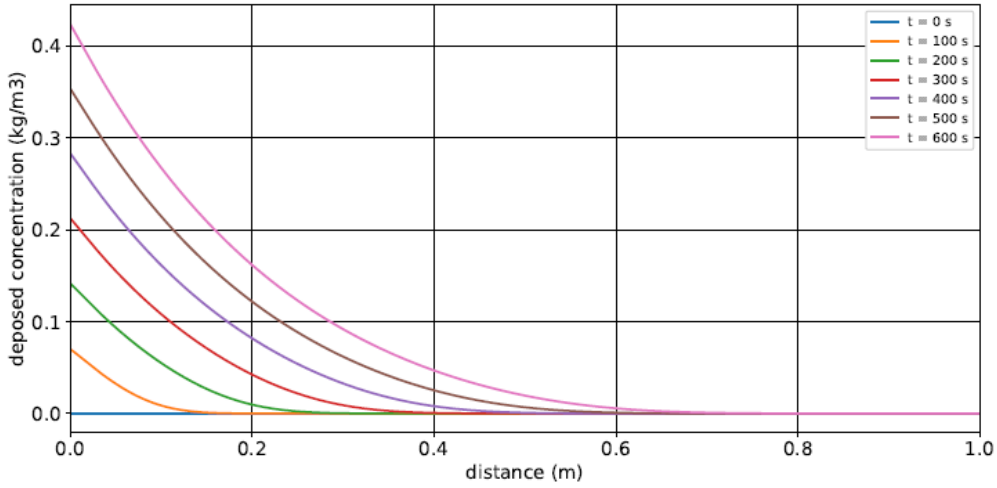

Figure 6-3 Particle deposition for a drinking water production well.

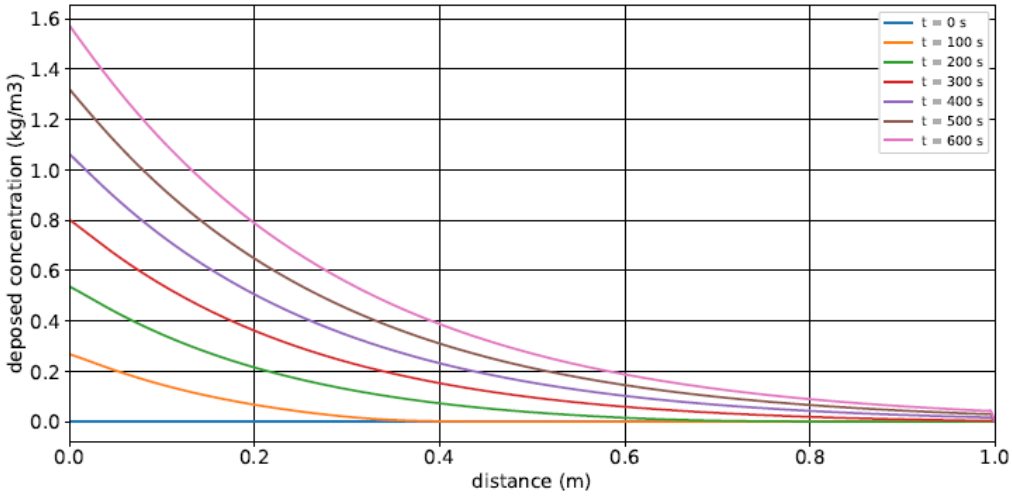

Figure 6-4 Particle deposition for a thermal storage system.

The simulations where made for a collision efficiency $\alpha = 0.1\,\mathrm{m}$ and damage coefficient $\beta = 0.1\,\mathrm{m}^3/\mathrm{kg}$. At this moment however there are no experimental measurement available that support these numbers and their temperature dependency is unknown.
The following steps are proposed in order to complete this preliminary research: extend the finite element implementation to an axi-symmetric 3D extended filtration model and make a simulation that supports the set-up of the laboratory experiment that are conducted by KWR.
Future research should focus on:

- back calculate KWR experiments,
- expand number of experiments for other soil types, temperatures and particle mixtures,
- examine the influence of mobilization of particles,
- investigate the effect of loaded mineral particles,
- examine effect of extra deposition of particles on the damage function due to thermal effect on the hydrochemical balance.

The three-dimensional version of the finite element code can then be used to check a real case HT-ATES system.

7 Bibliography

Bear, J. and A. Verruijt, 1987. Modeling Groundwater Flow and Pollution. Reidel.

De Zwart, A. H., 2007. Investigation of Clogging Processes in Unconsolidated Aquifers near Water Supply Wells. Ph.D. thesis, Delft University of Technology.

Diersch, H.-J. G., 2014. FEFLOW; Finite Element Modeling of Flow, Mass and Heat Transportin Porous and Fractured Media. Springer.

Rajagopalan, R. A. T. and C. Tien, 1976. “Trajectory Analysis of Deep-bed Filtration with the Sphere-in-Cell Porous Model.” AIChE Journal 22(3): 523-533.

Tufenkji, N. and M. Elimelech, 2004. “Correlation Equation for Predicting Single-Collector Efficiency in Physicochemical Filtration in Saturated Porous Media.” Environ Sci Technol 38(2): 529-536.

Tufenkji, N., J. A. Redman and M. Elimelech, 2003. “Interpreting deposition patterns of microbial particles in laboratory- scale column experiments.” Environ Sci Technol 37(3): 616-623.

Van Esch, J. M., 2010. Adaptive Multiscale Finite Element Method for Subsurface Flow Simulation. Ph.D. thesis, Delft University of Technology.

Vreugdenhill, C., 1989. Computational Hydraulics; An Introduction. Springer-Verlag.
Yao, K. M., T. Habibian, and C. O’Melia, 1971. “Water and Waste Water Filtration: Concepts and Applications.” Environmental Science and Technology 5(11): 1105-1112.

WARMINGUP
Innovatief Duurzaam Warmtecollectief

Adres
Princetonlaan 6
3584 CB Utrecht

Postadres
Postbus 80015
3508 TA Utrecht

Telefoon
088 866 42 56

E-mail
contact@warmingup.info

Website
www.warmingup.info

Versie 1 **10 augustus 2022**